7018 *Inorg. Chem.* **2009**, *48*, 7018–7025
DOI: 10.1021/ic900026c

Inorganic Chemistry
Article

Sodium Ion Mobility in Na_xCoO_2 ($0.6 < x < 0.75$) Cobaltites Studied by ^{23}Na MAS NMR

Dany Carlier,* Maxime Blangero, Michel Ménétrier, Michaël Pollet, Jean-Pierre Doumerc, and Claude Delmas

ICMCB, CNRS Université Bordeaux 1, 87 Av. du Dr. A. Schweitzer, 33608 Pessac Cedex, France

Received January 8, 2009

Various P2 and P′3-Na_xCoO_2 phases, with x ranging approximately from 0.6 to 0.75, have been studied by variable-temperature ^{23}Na magic angle spinning (MAS) NMR. Signal modification versus temperature plots clearly show that Na^+ ions are not totally mobile at room temperature on the NMR time scale. As the temperature increases, the line shape change of the ^{23}Na MAS NMR signal differs for the P2 and P′3 stackings and is interpreted by the differences of Na^+ ion sites and of sodium diffusion pathways in the two structures.

I. Introduction

In the 1980s, Na_xCoO_2 had been widely investigated as a potential electrode material for sodium batteries in our laboratory.[1−3] At that time, an unusually large thermoelectric power of 80 μV/K was measured for a polycrystalline metallic-like $Na_{0.7}CoO_2$ phase at 300 K.[3] More recently, the Na_xCoO_2 system has gained renewed interest because of its direct relevance to several condensed matter topics of great current interest for different x values: superconductivity when hydrated for $x \sim 0.3$,[4] complex $S = {}^1/_2$ magnetic orderings on a triangular matrix for $x \sim 0.7$,[5] and promising thermoelectric properties.[6,7] The P′3-Na_xCoO_2 ($x \sim 0.6$) phase is also interesting as a conductive additive for Ni−MH electrodes.[8] The Na_xCoO_2 system has been widely investigated in the low-temperature region; little is, however, known about the high-temperature behavior of this oxide family.

Depending on their synthesis conditions and sodium content, the Na_xCoO_2 phases can exhibit different alternate stackings of edge-sharing CoO_6 octahedra slabs and of partially vacant alkali layers. The packing sequences of the oxygen layers lead to different oxygen environments for the Na^+ ions (octahedral or prismatic) and to different numbers of CoO_2 sheets within the pseudohexagonal unit cell. These phases will be named in the following using the nomenclature previously proposed by Delmas et al. for the layered oxides:[9] the P or O letter describing the alkali ion site (prismatic or octahedral, respectively) is followed by a number (1, 2, 3, etc.) indicating the number of CoO_2 slabs within the hexagonal cell. Sometimes, the letter can be followed by a "prime" (like in P′3), which indicates a monoclinic distortion of the unit cell. In the present paper, we focus on the P2 and P′3-Na_xCoO_2 phases. Figure 1 shows the structures of these phases, highlighting the differences in the oxygen closed-packing sequences (ABBA... for P2 and ABBCCA... for P3) and in the resulting alkali prismatic environments.

P2-Na_xCoO_2 (Figure 1a) crystallizes in the hexagonal $P6_3/mmc$ space group and was previously reported for $0.64 < x < 0.74$,[10] and higher sodium concentrations were obtained by electrochemical intercalation.[1] More recently, the upper limit was reinvestigated by Huang et al., who reported that sodium content rates up to $x \approx 0.8$ could be obtained by direct powder synthesis but higher sodium concentrations could only be obtained by chemical intercalation.[11] In this structure, the Na^+ ions are distributed in two distinct prismatic sites labeled Na(1) and Na(2) in the literature: Na(1) shares only faces whereas Na(2) shares only edges with surrounding CoO_6 octahedra (Figure 1a). Recently, several groups reported sodium/vacancy-ordered

*To whom correspondence should be addressed. E-mail: carlier@icmcb-bordeaux.cnrs.fr.

(1) Delmas, C.; Braconnier, J. J.; Fouassier, C.; Hagenmuller, P. *Electrochem. Solid State Ionics* **1981**, *3−4* (Aug), 165–169.
(2) Molenda, J.; Delmas, C.; Hagenmuller, P. *Solid State Ionics* **1983** *9−10* (Dec), 431–435.
(3) Molenda, J.; Delmas, C.; Dordor, P.; Stoklosa, A. *Solid State Ionics* **1984**, *12* (Mar), 473–477.
(4) Takada, K.; Sakurai, H.; Takayama-Muromachi, E.; Izumi, F.; Dilanian, R. A.; Sasaki, T. *Nature (London)* **2003**, *422* (6927), 53–55.
(5) Foo, M. L.; Wang, Y. Y.; Watauchi, S.; Zandbergen, H. W.; He, T.; Cava, R. J.; Ong, N. P. *Phys. Rev. Lett.* 2004, 92 (24).
(6) Terasaki, I.; Sasago, Y.; Uchinokura, K. *Phys. Rev. B* **1997**, *56*, 12685.
(7) Lee, M.; Viciu, L.; Li, L.; Wang, Y. Y.; Foo, M. L.; Watauchi, S.; Pascal, R. A.; Cava, R. J.; Ong, N. P. *Nat. Mater.* **2006**, *5* (7), 537–540.
(8) Tronel, F.; Guerlou-Demourgues, L.; Basterreix, M.; Delmas, C. *J. Power Sources* **2006**, *158* (1), 722–729.
(9) Delmas, C.; Fouassier, C.; Hagenmuller, P. *Physica* **1980**, *99B*, 81.
(10) Fouassier, C.; Matejka, G.; Reau, J. M.; Hagenmuller, P. *J. Solid State Chem.* **1973**, 532.
(11) Huang, Q.; Foo, M. L.; Pascal, R. A.; Lynn, J. W.; Toby, B. H.; He, T.; Zandbergen, H. W.; Cava, R. J. *Phys. Rev. B* **2004**, *70* (18), 184110.

 Published on Web 05/06/2009 © 2009 American Chemical Society

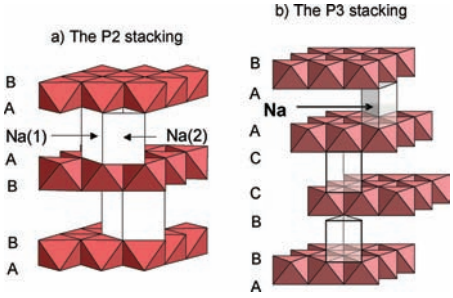

Figure 1. P2- and P3-type stackings of lamellar Na_xCoO_2 phases ($0.6 < x < 0.74$). Na^+ ions are not displayed for clarity.

structures in the P2-Na_xCoO_2 systems[12−17] and phase transition associated with an ordering/disordering of the Na^+ cations in the CoO_2 interslab.[18,19]

The room temperature monoclinic structure of P′3-Na_xCoO_2 ($x \sim 0.6$) has been precisely determined by X-ray diffraction (XRD):[20,21] the unit cell contains a single CoO_2 layer, and the space group is $C2/m$. Its stability domain was previously reported for $0.55 \leq x \leq 0.68$.[10] We recently showed that the P′3-$Na_{0.62}CoO_2$ phase undergoes a phase transition just above room temperature that is associated with an ordering/disordering of the Na^+ cations in the CoO_2 interslab space, which leads to a high-temperature rhombohedral P3-Na_xCoO_2 unit cell (space group $R3m$).[22] In P3-Na_xCoO_2 (Figure 1b), all of the Na^+ ions occupy a single type of prismatic site sharing a face with a CoO_6 octahedron on one side and edges with surrounding CoO_6 octahedra on the opposite side.

Few ^{23}Na and ^{59}Co magic angle spinning (MAS) NMR studies of sodium cobaltites have been reported so far: some of us studied the diamagnetic O3-$NaCoO_2$ phase,[23] and a full ^{23}Na MAS NMR study of the P′3-$Na_{0.6}CoO_2$ phase was also reported in our P′3/P3 phase transition paper.[22] Several research groups investigated some P2-Na_xCoO_2 phases using broad-line NMR-type spectrometers on either powders,[24−27] oriented powders,[28,29] or single crystals.[30] For example, low-temperature ^{23}Na NMR has shown that sodium ordering occurs for a specific phase $x \sim 0.7$, together with possible charge ordering[28] on cobalt ions. Actually, as the temperature increases, the magnetic susceptibility of the Na_xCoO_2 phases decreases, the NMR paramagnetic shifts decrease, and so does their difference for the various sites. The paramagnetic shift of the ^{23}Na NMR signal is mainly due to the Fermi contact interaction due to the electron spin transfer from cobalt ions to the sodium nucleus (see section IIb). Therefore, the resulting shift of the ^{23}Na NMR signal is weaker that the signal paramagnetic shift of cobalt nuclei themselves. High-resolution ^{23}Na NMR is then required in order to study the system around room temperature and above. In a recent ^{23}Na NMR study of a P2-$Na_{0.75}CoO_2$ phase, Julien et al. could get enough resolution at room temperature on single-crystal samples to observe two signals that they assigned to sodium motional averaging of ions with different mobilities within the interslab space.[30] For powder samples, MAS NMR is the most suitable technique for a study of the sodium cobaltites around room temperature and higher. With our experimental conditions, a resolution of a few parts per million could be obtained. In a similar way, ^7Li MAS NMR has already been used to study lithium paramagnetic layered oxides,[31−33] and ^{23}Na MAS NMR was used to study mobility in some diamagnetic samples like zeolites,[34] perovskites,[35] or Nasicon.[36] In this paper, we report variable-temperature (VT) ^{23}Na MAS NMR experiments in order to gain new insights into the sodium mobility in the interslab space of the P2 and P′3-Na_xCoO_2 phases.

II. Experimental Section

Sample Syntheses. Polycrystalline samples of P2-Na_xCoO_2, with nominal Na/Co ratios (x_0) of 0.55, 0.66, 0.77, and 0.88 have been prepared by direct powder synthesis in order to isolate phases in the thermodynamic $0.64 < x < 0.8$ range. The $x_0 = 0.55$ and 0.88 compositions are intentionally out of the existence domain ($0.64 < x < 0.74$) reported by Fouassier et al. in order to ensure that the limiting compositions are obtained.[10] Powders of Na_2CO_3 and Co_3O_4 were thoroughly ground in a mortar and fired at 873 K for 12 h. The sample was subsequently reground and sintered at 1173 K in a dry oxygen flow for 24 h.

Likewise, the synthesis of polycrystalline powders of P′3-Na_xCoO_2 ($x \sim 0.62$) was performed using a conventional solid-state route starting from powders of Na_2O and Co_3O_4 intimately mixed under argon in a glovebox and heated for 12 h at 823 K under a dry oxygen flow.

The final products were slowly cooled at 1 K/min and immediately stored in an argon-filled glovebox to prevent

(12) Zandbergen, H. W.; Foo, M.; Xu, Q.; Kumar, V.; Cava, R. J. *Phys. Rev. B* 2004, 70 (2).
(13) Williams, A. J.; Attfield, J. P.; Foo, M. L.; Viciu, L.; Cava, R. J. *Phys. Rev. B* **2006**, 73.
(14) Roger, M.; Morris, D. J. P.; Tennant, D. A.; Gutmann, M. J.; Goff, J. P.; Hoffmann, J. U.; Feyerherm, R.; Dudzik, E.; Prabhakaran, D. Boothroyd, A. T.; Shannon, N.; Lake, B.; Deen, P. P. *Nature (London)* **2007**, *445* (7128), 631–634.
(15) Zhou, S.; Wang, Z. *Phys. Rev. Lett.* **2007**, *98* (22), 226402.
(16) Yang, H. X.; Nie, C. J.; Shi, Y. G.; Yu, H. C.; Ding, S.; Liu, Y. L.; Wu, D.; Wang, N. L.; Li, J. Q. *Solid State Commun.* **2005**, *134* (6), 403–408.
(17) Shu, G. J.; Prodi, A.; Chu, S. Y.; Lee, Y. S.; Sheu, H. S.; Chou, F. C. *Phys. Rev. B* **2007**, *76*, 184115.
(18) Igarashi, D.; Miyazaki, Y.; Yubuta, K.; Kajitani, T. *Jpn. J. Appl. Phys., Part 1* **2007**, *46* (1), 304–310.
(19) Igarashi, D.; Miyazaki, Y.; Kajitani, T.; Yubuta, K. *Phys. Rev. B* **2008**, *78*, 184112.
(20) Ono, Y.; Ishikawa, R.; Miyazaki, Y.; Ishii, Y.; Morii, Y.; Kajitani, T. *J. Solid State Chem.* **2002**, *166* (1), 177–181.
(21) Viciu, L.; Bos, J. W. G.; Zandbergen, H. W.; Huang, Q.; Foo, M. L.; Ishiwata, S.; Ramirez, A. P.; Lee, M.; Ong, N. P.; Cava, R. J. *Phys. Rev. B* **2006**, *73*, 174104.
(22) Blangero, M.; Carlier, D.; Pollet, M.; Darriet, J.; Delmas, C.; Doumerc, J. P. *Phys. Rev. B* **2008**, *77* (18), 184116.
(23) Siegel, R.; Hirschinger, J.; Carlier, D.; Menetrier, M.; Delmas, C. *Solid State Nucl. Magn. Reson.* **2003**, *23* (4), 243–262.
(24) Stallworth, P.; Greenbaum, S.; Ma, Y.; Ding, L.; Doeff, M.; Visco, S. *Solid State Ionics* **1996**, *86−8*, 797–803.
(25) Ray, R.; Ghoshray, A.; Ghoshray, K. *Phys. Rev. B* **1999**, *59* (14), 9454–9461.
(26) Gavilano, J. L.; Rau, D.; Pedrini, B.; Hinderer, J.; Ott, H. R.; Kazakov, S. M.; Karpinski, J. *Phys. Rev. B* **2004**, *69*, 100404(R).
(27) Gavilano, J. L.; Pedrini, B.; Magishi, K.; Hinderer, J.; Weller, M.; Ott, H. R.; Kazakov, S. M.; Karpinski, J. *Phys. Rev. B* **2006**, *74*, 064410.
(28) Mukhamedshin, I. R.; Alloul, H.; Collin, G.; Blanchard, N. *Phys. Rev. Lett.* **2004**, *93*, 167601.
(29) Alloul, H.; Mukhamedshin, I. R.; Collin, G.; Blanchard, N. *Europhys. Lett.* **2008**, *82* (1), 17002.
(30) Julien, M. H.; de Vaulx, C.; Mayaffre, H.; Berthier, C.; Horvatic, M.; Simonet, V.; Wooldridge, J.; Balakrishnan, G.; Lees, M. R.; Chen, D. P.; Lin, C. T.; Lejay, P. *Phys. Rev. Lett.* **2008**, *100* (9), 096405.
(31) Menetrier, M.; Saadoune, I.; Levasseur, S.; Delmas, C. *J. Mater. Chem.* **1999**, *9* (5), 1135–1140.
(32) Carlier, D.; Menetrier, M.; Delmas, C. *J. Mater. Chem.* **2001**, *11* (2), 594–603.
(33) Grey, C. P.; Dupre, N. *Chem. Rev.* **2004**, *104* (10), 4493–4512.
(34) Lim, K. H.; Grey, C. P. *J. Am. Chem. Soc.* **2000**, *122* (40), 9768–9780.
(35) Kotecha, M.; Chaudhuri, S.; Grey, C. P.; Frydman, L. *J. Am. Chem. Soc.* **2005**, *127* (47), 16701–16712.
(36) Losilla, E. R.; Aranda, M. A. G.; Bruque, S.; Paris, M. A.; Sanz, J.; West, A. R. *Chem. Mater.* **1998**, *10* (2), 665–673.

moisture contamination. Sample preparation for XRD and NMR experiments has also been performed in the glovebox.

XRD. XRD patterns were recorded with a Philips X'Pert Pro powder diffractometer in the Bragg−Brentano geometry, using Co Kα radiation. The data collection was made in the 10−120° 2θ range with a 0.0167° step, using an X'Celerator detector (linear particle size distribution covering 2.122 mm equivalent to a typical counting time of 200 s/step). The powder was kept in an airtight holder under dry argon to prevent any reaction with air moisture. The diffraction data were processed by means of the *Fullprof* program. [37]

^{23}Na NMR. Single-pulse ^{23}Na MAS NMR spectra were recorded on a Bruker 300 Avance spectrometer at 79.403 MHz. VT NMR experiments were carried out in the 268−475 K range using a Bruker 4 mm WVT MAS probe. A spinning speed of 13 Hz was used. Polycrystalline samples were mixed with dry silica (typically in a 1:1 weight ratio), in order to facilitate the spinning and improve the field homogeneity, because the samples may exhibit metallic or paramagnetic-like properties. The mixture was placed in zirconia rotors in a drybox. No change in the NMR signal was observed even for rotors kept several days out of the drybox, indicating satisfactory airtightness of the cell. Because ^{23}Na is a quadrupolar nucleus with $I = {}^3/_2$, a short pulse length of 1 μs corresponding to a selective $\pi/12$ pulse determined using an aqueous 0.1 mol/L NaCl solution was employed. In these conditions, we ensure that the main signal observed is due to the $-{}^1/_2 \rightarrow +{}^1/_2$ central transition. The spectral width was set to 1 MHz, and the recycle time $D_0 = 0.5$ s is long enough to avoid T_1 relaxation time saturation effects with 1600 scans per spectrum. The baseline distortions resulting from the spectrometer dead time (5−10 μs) were computationally removed using a polynomial baseline correction routine. The external reference was a 0.1 mol/L NaCl aqueous solution.

III. Results and Discussion

1. Structural Properties and Composition of the Na_xCoO_2 Phases. a. P2-Na_xCoO_2 Phases. Figure 2a shows the XRD patterns of the various P2-Na_xCoO_2 samples. As expected, samples of which the starting compositions x_0 were out of the range of stability of the P2 phase published by Fouassier et al. contain impurities such as sodium diamagnetic compounds evidenced by ^{23}Na NMR and Co_3O_4 seen by XRD. Note that the latter does not affect the ^{23}Na MAS NMR signals. Another implication is that bulk composition determinations, e.g., by means of inductively coupled plasma (ICP) measurements, are not reliable for these samples.

An increasing number of reports correlate the room temperature *c*-axis parameter value to the sodium content *x*. [11,17,38,39] The increase of the *c*-axis lattice parameter with decreasing sodium content indeed results from an increasing Coulombic repulsion between CoO_2 layers. Knowing the evolution of *x* as a function of *c* therefore provides a dependable and convenient way to determine the sodium content from an XRD data set. The refined *c*-axis lattice parameters of the various P2 samples are summarized in Table 1.

Two previous series of data were used: experimental data reported by Shu et al. for single crystals[17] and theoretical values obtained from the first-principles geometry optimization of ordered sodium/vacancy phases.[39] Both results give a linear relationship between *c* and *x*.

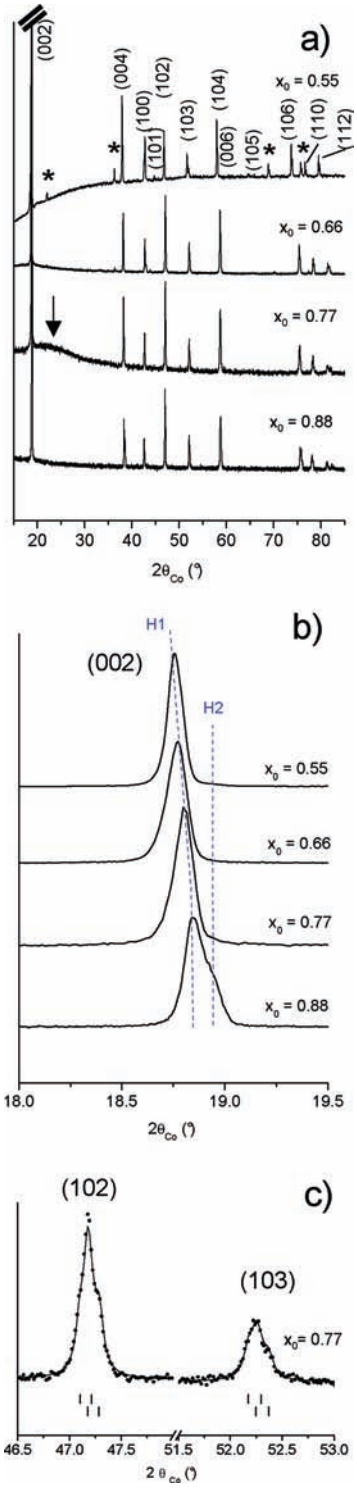

Figure 2. (a) XRD patterns of the P2-Na_xCoO_2 phases for various nominal Na/Co ratios (x_0). Peaks marked with asterisks correspond to Co_3O_4. The broad peak indicated by the arrow for the $x_0 = 0.77$ sample is due to silica mixed with the sample in order to improve the NMR rotor spinning. (b) Expansion of the (002) diffraction line for the P2 samples. (c) Expansion of the (102) and (103) diffraction lines for the P2 phase prepared with $x_0 = 0.77$ showing the presence of two phases in the material. The vertical lines correspond to the positions of the diffraction lines due to Co $K\alpha_1$ and $K\alpha_2$ radiation for both phases.

For the $x = 0.55$ sample, the calculated Na/Co value is higher than the nominal one, in agreement with the observation of Co_3O_4 by XRD (Figure 2a). It is also close to the lower bound of the stability range of 0.64 reported

(37) Rodriguez-Carvajal, J. *Phys. B: Condens. Matter* **1993**, *192*, 55.
(38) Meng, Y. S.; Hinuma, Y.; Ceder, G. *J. Chem. Phys.* 2008, 128 (10).
(39) Hinuma, Y.; Meng, Y. S.; Ceder, G. *Phys. Rev. B* 2008, 77 (22).

Table 1. Cell Parameter Values Obtained for the P2-Na_xCoO_2 Samples as a Function of the Nominal Na/Co Ratio (x_0)[a]

nominal sodium content x_0		a (Å)	c (Å)	x sodium content based on c axis value calculations [39]	x sodium content based on the c axis value from single crystal analysis[17]
0.88	two phases	2.835(1)	10.862(1)	0.712	0.77
		2.838(1)	10.808(1)	0.749	0.812
0.77	two phases	2.835(1)	10.895(1)	0.689	0.742
		2.831(1)	10.887(1)	0.694	0.749
0.66	one phase	2.829(1)	10.917(1)	0.673	0.722
0.55	one phase	2.827(1)	10.947(1)	0.652	0.693

[a] The sodium content x has been determined from the linear x dependence of the c parameter taken either from ab initio calculations[39] or from experimental studies.[17]

by Fouassier et al. The Na/Co ratios of the other samples are close to or smaller than the initial one. For $x_0 = 0.88$, the Na/Co value is much smaller than the nominal one, in agreement with the stability domain given in the literature.[40] However, for this sample, no impurities that would contain the extra sodium were seen by XRD. Taking into account the difficulty in determining accurately the sodium rate in our samples, we will keep the designation of the samples by their nominal Na/Co ratio x_0 noted in brackets in the formula $Na_{\text{“}x0\text{”}}CoO_2$. Because the main aspect of our study is a comparison of the Na^+ ion mobility in P2 and P'3 samples, the exact sodium content is not a critical parameter, and different P2-Na_xCoO_2 samples exhibit similar behavior, as shown later.

Among the selected samples, a single P2 phase is obtained for $x_0 = 0.55$ and 0.66 nominal compositions, whereas a mixture of two P2 phases is obtained for $x_0 = 0.77$ and 0.88. For $x_0 = 0.77$, the ^{23}Na MAS NMR spectra (shown later) clearly indicated two phases, which is confirmed by a careful look at the shape of the (102) and (103) XRD peaks (Figure 2c) that are better fitted with two P2 components. The two phases should exhibit a small difference in the sodium composition that is accompanied by a subtle change in the unit cell parameters (Table 1). In contrast, XRD analysis of the $Na_{\text{“}0.88\text{”}}CoO_2$ sample clearly shows two P2 phases whose c parameter values significantly differ, as indicated by the splitting of the (002) diffraction line (Figure 2b). From the measured cell parameter values and from the sodium amount estimated around 0.75, these two phases should correspond to the so-called H1 + H2 phases reported by Huang et al. that exhibit a P2 stacking with different cell parameters and slightly different sodium positions in the interslab space.[40]

b. P′3 and P3-Na_xCoO_2 Phases. XRD analysis of the P′3 phase and the high-temperature phase transition have been detailed elsewhere.[22] A nominal Na/Co ratio of 0.66 was used. Because no impurities were seen by XRD and only traces of diamagnetic sodium compounds was observed by NMR, we performed ICP-atomic emission spectroscopy (AES) analysis of the product, which leads to the raw formula $Na_{0.62}CoO_2$. Because byproduced sodium oxides are highly volatile, it is not surprising to obtain a final lower Na/Co ratio. Table 2 summarizes the corresponding cell parameters at room temperature and 393 K. As the temperature increases, the phase undergoes a structural transition to an undistorted P3 phase that is driven by the disordering of Na^+ ions.

Table 2. Cell Parameters of the Monoclinic P′3-$Na_{0.62}CoO_2$ at Room Temperature and of the Rhombohedral P3-$Na_{0.62}CoO_2$ at 393 K

	P′3-$Na_{0.62}CoO_2$ at RT	P3-$Na_{0.62}CoO_2$ at 393 K
space group	$C2/m$ ($Z = 2$)	$R3m$ ($Z = 3$)
cryst syst	monoclinic	rhombohedral
a (Å)	4.8995(6)	2.8276(2)
b (Å)	2.8263(2)	2.8276(2)
c (Å)	5.7155(5)	16.518(3)
β (deg)	106.069(6)	

2. ^{23}Na MAS NMR Study. a. NMR Line Shape. Figure 3 shows the MAS NMR spectra of the P2-$Na_{\text{“}x0\text{”}}CoO_2$ samples ($x_0 = 0.55$, 0.66, 0.77, and 0.88) and of the P′3-$Na_{0.62}CoO_2$ one. The MAS NMR technique allows (for infinite spinning speed) averaging of both of first-order quadrupolar and nuclear dipolar interactions, mainly responsible for the broadening of the NMR lines experienced in solid-state NMR experiments. However, for nuclei with a strong quadrupolar constant like ^{23}Na, located on a site with noncubic symmetry, a broad signal remains because of the second-order quadrupolar interaction that is affected, but not suppressed, by MAS. At room temperature, the Na_xCoO_2 phases exhibit such a ^{23}Na MAS NMR signal located around 350 ppm. A set of spinning side bands are also observed on both sides of this signal. Another signal located around 0 ppm, with a slightly longer T_1 spin−lattice relaxation time, is also observed and assigned to diamagnetic sodium impurities that are not seen by XRD. This feature could be attributed to sodium carbonates because the impurity amount increases with x_0. For $x_0 = 0.88$, the presence of larger amounts of the sodium-containing diamagnetic impurity is consistent with a nominal sodium content that exceeds the upper limit of the P2 phase domain.

At room temperature, the P2-$Na_{\text{“}0.55\text{”}}CoO_2$, P2-$Na_{\text{“}0.66\text{”}}CoO_2$, and P′3-$Na_{0.62}CoO_2$ single phases exhibit signals with clear second-order quadrupolar line shape and with a broadening due to a distribution of sodium environments. Indeed, the spectra cannot be fitted satisfactorily with a single line, even with strong dipolar broadening, as could be expected for paramagnetic samples. The origin of this distribution is not clear: it can be due to complex sodium/vacancy ordering (possibly with a modulation), which can be associated with a possible displacement of the alkaline ion from the center of the

(40) Huang, Q.; Khaykovich, B.; Chou, F. C.; Cho, J. H.; Lynn, J. W.; Lee, Y. S. *Phys. Rev. B* 2004, 70 (13).

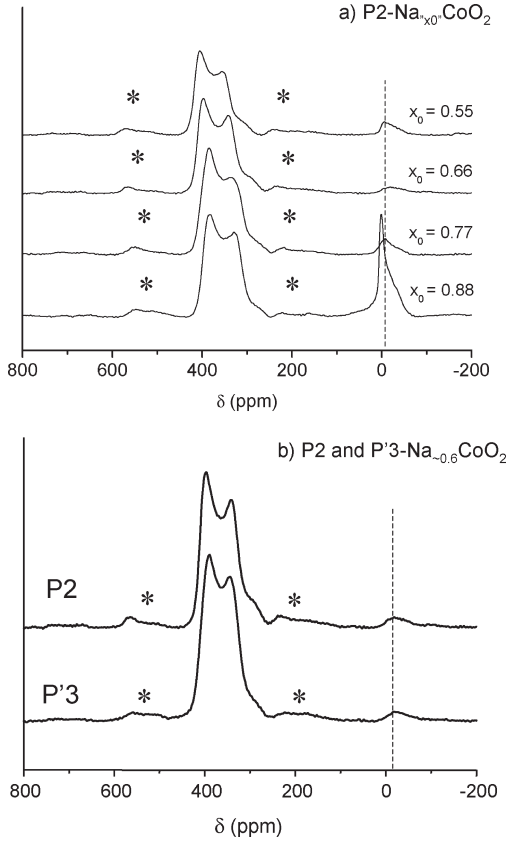

Figure 3. (a) Room temperature ^{23}Na MAS NMR spectra of the P2-Na_xCoO_2 samples for various nominal Na/Co ratios (x_0). (b) ^{23}Na MAS NMR spectra recorded for P2 and P′3-Na_xCoO_2 samples with close sodium contents ($x \sim 0.6$). The dashed line indicates the contribution of diamagnetic impurities. Spinning side bands are indicated by asterisks.

prismatic sites, as was already observed for the P2 and P′3-Na_xCoO_2 phases[22,41,42] and for the P2-$K_{0.57}CoO_2$ phase.[43] This sodium ordering could also be associated with a charge ordering in the cobalt layers. Therefore, many different sodium environments can exist with no real chemical exchange between them on the NMR time scale, at least at room temperature.

b. Line Shifts versus *x*. Figure 3 shows that the MAS NMR signal position depends on the sodium content. The smaller the Na^+ content, the more cobalt ions are formally oxidized to paramagnetic Co^{4+} and the more this signal is shifted to larger values. The shift dependence versus temperature, as detailed in the next paragraph, is typical of paramagnetic samples with a Fermi contact shift, in agreement with the Curie−Weiss magnetic properties of Na_xCoO_2 phases.[5] Because the shifts of P′3-$Na_{0.62}CoO_2$ and P2-$Na_{"0.66"}CoO_2$ are very similar, the spin concentration should be close in both samples and the spin-transfer mechanism from the paramagnetic transition-metal ion to the sodium nucleus should occur through similar mechanisms. The Na_xCoO_2 phases exhibit both a metallic electrical conductivity and Curie−Weiss paramagnetism, whose origin is still unclear. Therefore, a (real) Knight shift-type contribution to the NMR shift is also expected, but there is no evidence for this.

c. Variable-Temperature Measurements: Na^+ Motion. Comparison between P2 and P′3-Na_xCoO_2 ($x \sim 0.6$). Figure 4 shows that the MAS NMR signal changes versus temperature for the three single phases prepared in this study, i.e, P2-$Na_{"0.55"}CoO_2$, P2-$Na_{"0.66"}CoO_2$, and P′3-$Na_{0.62}CoO_2$. As the temperature increases, the isotropic shift decreases, like the susceptibility, denoting a Fermi contact mechanism. However, the heating effects on the shape of the signal for the P2 and P′3 phases are completely different.

For the P2 phases (Figure 4a,b), a temperature increase results in a sharpening of the signal that finally exhibits at 475 K a well-defined second-order line shape and would exhibit a ^{23}Na nucleus in a unique site with axial symmetry of the electric field gradient (EFG). This signal modification can be interpreted by the Na^+ ion motion in the interslab space that is not fully achieved at room temperature compared to the NMR time scale and increases as the temperature increases, leading to an averaged single ^{23}Na NMR signal. For the signals recorded at 475 K, a fit of the line could be done and the results are reported in Table 3.

For the P′3-$Na_{0.62}CoO_2$ phase (Figure 4c), a temperature increase results in a gradual collapse of the second-order quadrupolar line shape and in the emergence of a narrower central resonance without second-order quadrupolar shape, as is expected for a $^{23}Na^+$ ion in a highly symmetric environment with weak or no EFG. These observations are also interpreted by the motion of the Na^+ cations in the interslab space on the time scale of NMR spectroscopy.

For all of the phases, upon cooling, the exact opposite effects are observed and the spectra recorded at room temperature at the end of the experiment are similar to those recorded before heating, indicating a good reversibility of the phenomenon.

In the following, we discuss the origin of the different effects of the Na^+ ion mobility as the temperature increases in the P2 and P3 stacking in relation to the Na^+ sites and the motion pathway in the interslab space for the two stackings, depicted in Figure 5.

In the P2 structure, Na^+ ions can be located on two different prismatic sites, Na(1) and Na(2), as was previously described. Each site has its own EFG values, with the main contribution to the principal axis system (V_{zz}) oriented along the *c* axis,[28] and is symmetric versus the middle of the interslab space. While moving, Na^+ ions migrate through the faces of the prisms and have to go from one type of Na site to the other one because each Na site is surrounded by three sites of the other type. In the structure, both Na(1) and Na(2) sites have a 3-fold axial symmetry with the same axis direction and therefore with the same direction of the main contribution to the principal axis system. A complete sodium chemical exchange leads to an averaged sodium signal that keeps a second-order line shape with axial symmetry, but with an averaged

(41) Huang, Q.; Lynn, J. W.; Toby, B. H.; Foo, M. L.; Cava, R. J. *J. Phys.: Condens. Matter* **2005**, *17* (12), 1831–1840.
(42) Viciu, L.; Huang, Q.; Cava, R. J. *Phys. Rev. B* **2006**, *73* (21), 212107.
(43) Blangero, M.; Decourt, R.; Carlier, D.; Ceder, G.; Pollet, M.; Doumerc, J. P.; Darriet, J.; Delmas, C. *Inorg. Chem.* **2005**, *44* (25), 9299–9304.

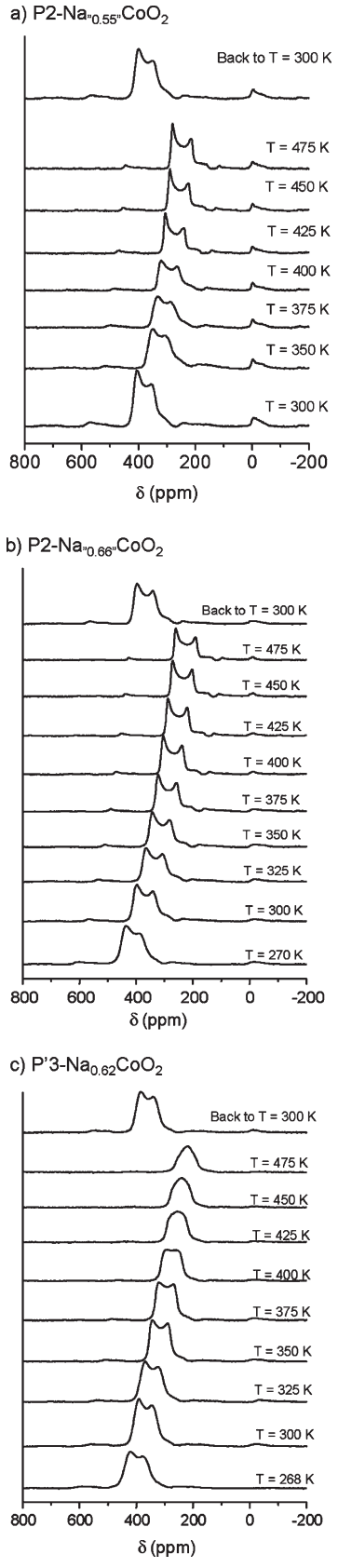

Figure 4. ^{23}Na MAS NMR spectra recorded as a function of temperature for the single phases: (a) P2-Na$_{"0.55"}$CoO$_2$; (b) P2-Na$_{"0.66"}$CoO$_2$; (c) P′3-Na$_{0.62}$CoO$_2$.

value of the main contribution V_{zz} between those of Na(1) and Na(2) sites.

Table 3. NMR Parameters for P2-Na$_x$CoO$_2$ Samples Determined from Fitting Spectra Recorded at 475 K for x_0 = 0.55, 0.66, and 0.88 and at 450 K for x_0 = 0.77[a]

nominal x_0	0.55	0.66	0.77		0.88
δ_{iso} (ppm)	304(1)	286(1)	293(1)	282(1)	272(1)
ν_Q (MHz)	1.93(1)	1.99(1)	1.98(1)	2.01(1)	2.03(1)

[a] $\eta \sim 0$ for all fits. Uncertainties on the fitted parameters are also given.

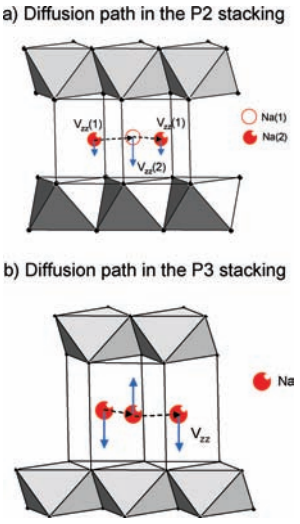

Figure 5. Drawing describing the Na$^+$ ion motion path in the interslab space for both P2 and P3 stacking involving different sodium prismatic sites. The direction of V_{zz} is not known but is schematically represented here in order to show that the two V_{zz} values for adjacent Na sites (i) have to be opposite in direction along z with the same magnitude for the P3 stacking and (ii) are not necessarily opposite but have different magnitudes for the P2 stacking.

In the P′3 (or P3) structure, adjacent prismatic Na sites are equivalent in the *ab* plane but antisymmetric in the *c* direction (Figure 5b), which is the direction of the main contribution to the EFG tensor. Therefore, we expect for these two sites similar V_{zz} magnitudes but with opposite directions along z. The mobility of the Na$^+$ cations in this phase thus result, by a chemical exchange phenomenon, in a cancelation of the V_{zz} contribution and therefore in a signal narrowing and suppression of the second-order line shape. Because the Na$^+$ ion mobility implies sites with axial symmetry and the fact that the trace of the quadrupolar interaction tensor is equal to zero, necessarily the averaged V_{xx} and V_{yy} contributions should be equal to zero and the final exchanged signal should be purely Lorentzian. However, we could not increase further the temperature with our experimental setup and stopped therefore at 475 K, where complete exchange is not reached.

The P′3−P3 phase transition that occurs near 350 K[22] does not correspond to an abrupt change in the ^{23}Na signal but to a progressive modification from a second-order line shape into a symmetric site line shape. This progressive evolution is also observed for the P′3 phase; therefore, the Na$^+$ ion mobility increase expected when the temperature increases leads to a progressive cancelation of the V_{zz} main EFG term.

Theoretical treatment of the evolution of the second-order quadrupolar line shape as a function of the EFG parameters of the sites and the pathways involved in the

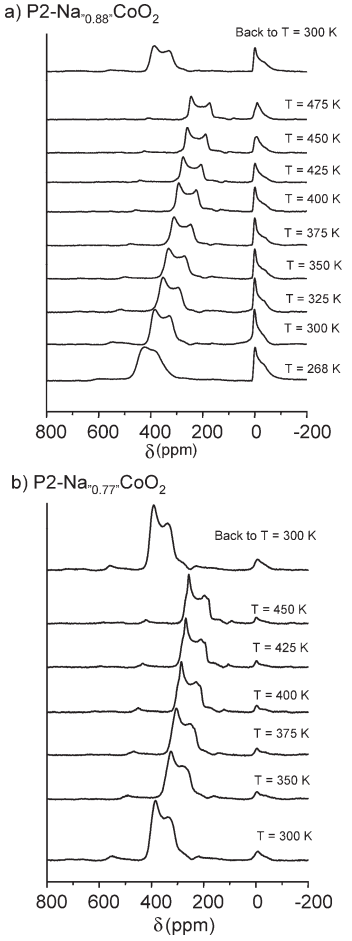

Figure 6. ^{23}Na MAS NMR spectra recorded as a function of the temperature for the nonpure samples: (a) P2-$Na_{0.88}CoO_2$; (b) P2-$Na_{0.77}CoO_2$.

ionic motion is in progress, in order to ensure our interpretation. Such numerical simulations were recently done on several diamagnetic inorganic samples by a few groups.[35,44−47]

Two-Phase Samples P2-Na_xCoO_2 (x_0 = 0.77 and 0.88). For two nominal sodium compositions, we obtained two-phase samples: for x_0 = 0.88, the XRD data are refined with two phases corresponding to H1 + H2 that Huang et al. reported,[41] and for x_0 = 0.77, the XRD pattern is better fitted with two P2 phases with really close cell parameters.

Figure 6 shows the evolution of the NMR line versus temperature. As for the other P2 phases, a temperature increase results in a sharpening of the signal that finally exhibits at 475 K a well-defined second-order line shape of an exchanged sodium between the Na(1) and Na(2) sites. At room temperature, one would have expected to observe the two contributions due to each P2 phase for both the x_0 = 0.77 and 0.88 samples. However, the second-order line shape signals are broadened by the sodium nucleus environment distribution so that the two components are not clearly seen. In contrast, for higher temperature, as the Na^+ ion mobility increases, the signals become sharper and the two contributions can be seen. In their study, Huang et al. reported that the H1 + H2 system undergoes a phase transition at 340 K to an H1 phase.[41] Following their work, the complex shape of the spectra of the P2-$Na_{0.88}CoO_2$ sample recorded at 268 K should be due to the presence of both H1 and H2 phases; as the temperature increases, this sample should undergo this structural transition and a unique well-defined averaged signal is recorded in our study. In contrast to the P2-$Na_{0.77}CoO_2$ sample, the two components are clearly observed at 450 K, evidencing that this sample remains biphased in our temperature range and therefore does not correspond to the H1 + H2 phase previously described. The spectra recorded at 450 K can be satisfactorily fitted with two components with a second-order quadrupolar interaction line shape (Figure 7). The fit parameters are discussed in the next section together with the ones of other P2 phases.

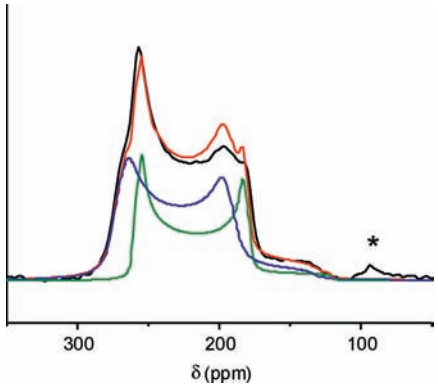

Figure 7. Decomposition of the central line of the ^{23}Na MAS NMR spectra of P2-$Na_{0.77}CoO_2$ recorded at 450 K including two second-order quadrupolar components (green and blue lines). Black line: experimental data. Red line: sum of the two fitted contributions. The fit parameters are given in Table 3.

d. Discussion on the Quadrupolar Constant Values. In Table 3 are listed the quadrupolar constants (ν_Q) determined from curve fittings[48] for the various P2-Na_xCoO_2 samples at 475 K for x_0 = 0.55, 0.66, and 0.88 and at 450 K for x_0 = 0.77. For the fits, a line shape typical of a second-order quadrupolar interaction with possible Gaussian broadening of the central $-^1/_2 \rightarrow +^1/_2$ transition in the fast MAS limit was used. V_{xx}, V_{yy}, and V_{zz} are the eigenvalues of the quadrupolar interaction tensor in the principal axis system. All of the fits lead to an anisotropy $\eta = (V_{yy} - V_{xx})/V_{zz}$ value very close to zero, i.e., a site with nearly axial symmetry. The isotropic position and the quadrupolar constant value were also obtained from these fits. The quadrupolar constant value $\nu_Q = eQV_{zz}/h$ is proportional to the principal axis value V_{zz} of the EFG tensor around the sodium nucleus (Q is the nuclear quadrupolar moment). As x decreases, the average ν_Q value decreases as the cell parameter a decreases and c increases

(44) Chu, P. J.; Gerstein, C. *J. Chem. Phys.* **1989**, *90* (7), 3713–3727.
(45) Kristensen, J. H.; Farnan, I. *J. Magn. Reson.* **2002**, *158*, 99–125.
(46) Kristensen, J. H.; Farnan, I. *J. Chem. Phys.* **2001**, *114* (21), 9608–9624.
(47) Schurko, R. W.; Wi, S.; Frydman, L. *J. Phys. Chem. A* **2002**, *106* (1), 51–62.
(48) Massiot, D.; Fayon, F.; M., C.; King, I.; Le Calvé, S.; Alonso, B.; Durand, J.-O.; Bujoli, B.; Gan, Z.; Hoatson, G. *Magn. Reson. Chem.* **2002**, *40*, 70–76.

(Table 1). The average ν_Q values obtained at 475 K for our P2 samples are similar to the values reported by Julien et al. for the six ^{23}Na signals recorded at 59 K on a $Na_{0.75}CoO_2$ single crystal ($\nu_Q \sim 1.9$ MHz)[30] but slightly higher than those reported for the three Na sites recorded at 100 K on a $Na_{0.66}CoO_2$ single crystal by Mukhamedshin et al. (ν_Q between 1.645 and 1.86 MHz)[28] or for a $Na_{0.7}CoO_2$ powder at room temperature reported by Gavilano et al. ($\nu_Q \sim 1.65$ MHz).[26] The comparison of the quadrupolar coupling constants obtained on our P2-Na_xCoO_2 samples with the literature is not straightforward because the sample compositions and the temperatures of the experiments differ. In our study, the evolution of the line shape with the temperature for pure P2 phases shows that ν_Q increases upon heating: at first sight, this is rather surprising because the sodium mobility is thermally activated and should lead to a narrowing of the signal if the cell parameters do not change. However, thermal expansion (both *c* and *a* are increasing) can largely modify the averaged EFG parameters around the sodium nucleus.

IV. Conclusions

With VT ^{23}Na MAS NMR measurements on various P2-Na_xCoO_2, with x ranging approximately from 0.6 to 0.75, and P′3-Na_xCoO_2 ($x = 0.62$), we showed that Na^+ ions are not totally mobile at room temperature on the NMR time scale. As the temperature increases, the change of the NMR line shape is significantly different for the two types of stackings. This result is interpreted by the difference in the geometry of the Na^+ sites in the two stackings (P2 and P3) and in the diffusion path in the interslab space of these structures. Some of the samples exhibit two P2 phases with very close sodium contents and cell parameters that were evidenced by MAS NMR only at high temperature, when the ionic mobility sharpens enough the second-order quadrupolar line shape.

Acknowledgment. The authors thank Marc-Henri Julien and Laurent Le Polles for fruitful discussions. Région Aquitaine and ANR-OCTE are acknowledged for financial support.